JACS
JOURNAL OF THE AMERICAN CHEMICAL SOCIETY
Article
pubs.acs.org/JACS

Exploring the Electron Transfer Pathways in Photosystem I by High-Time-Resolution Electron Paramagnetic Resonance: Observation of the B-Side Radical Pair $P_{700}^{+}A_{1B}^{-}$ in Whole Cells of the Deuterated Green Alga *Chlamydomonas reinhardtii* at Cryogenic Temperatures

Thomas Berthold,[†] Erika Donner von Gromoff,[‡] Stefano Santabarbara,[§,⊥] Patricia Stehle,[†] Gerhard Link,[†] Oleg G. Poluektov,[∥] Peter Heathcote,[§] Christoph F. Beck,[‡] Marion C. Thurnauer,[∥] and Gerd Kothe*[,†]

[†]Department of Physical Chemistry, University of Freiburg, Albertstrasse 21, 79104 Freiburg, Germany

[‡]Faculty of Biology, University of Freiburg, Schaenzlestrasse 1, 79104 Freiburg, Germany

[§]School of Biological and Chemical Sciences, Queen Mary University of London, Mile End Road, London E1 4NS, United Kingdom

[∥]Chemical Sciences and Engineering Division, Argonne National Laboratory, 9700 South Cass Avenue, Argonne, Illinois 60439, United States

Supporting Information

ABSTRACT: Crystallographic models of photosystem I (PS I) highlight a symmetrical arrangement of the electron transfer cofactors which are organized in two parallel branches (A, B) relative to a pseudo-C_2 symmetry axis that is perpendicular to the membrane plane. Here, we explore the electron transfer pathways of PS I in whole cells of the deuterated green alga *Chlamydomonas reinhardtii* using high-time-resolution electron paramagnetic resonance (EPR) at cryogenic temperatures. Particular emphasis is given to quantum oscillations detectable in the tertiary radical pairs $P_{700}^{+}A_{1A}^{-}$ and $P_{700}^{+}A_{1B}^{-}$ of the electron transfer chain. Results are presented first for the deuterated site-directed mutant PsaA-M684H in which electron transfer beyond the primary electron acceptor A_{0A} on the PsaA branch of electron transfer is impaired. Analysis of the quantum oscillations, observed in a two-dimensional Q-band (34 GHz) EPR experiment, provides the geometry of the B-side radical pair. The orientation of the **g** tensor of P_{700}^{+} in an external reference system is adapted from a time-resolved multifrequency EPR study of deuterated and ^{15}N-substituted cyanobacteria (Link, G.; Berthold, T.; Bechtold, M.; Weidner, J.-U.; Ohmes, E.; Tang, J.; Poluektov, O.; Utschig, L.; Schlesselman, S. L.; Thurnauer, M. C.; Kothe, G. *J. Am. Chem. Soc.* **2001**, *123*, 4211−4222). Thus, we obtain the three-dimensional structure of the B-side radical pair following photoexcitation of PS I in its native membrane. The new structure describes the position and orientation of the reduced B-side quinone A_{1B}^{-} on a nanosecond time scale after light-induced charge separation. Furthermore, we present results for deuterated wild-type cells of *C. reinhardtii* demonstrating that both radical pairs $P_{700}^{+}A_{1A}^{-}$ and $P_{700}^{+}A_{1B}^{-}$ participate in the electron transfer process according to a mole ratio of 0.71/0.29 in favor of $P_{700}^{+}A_{1A}^{-}$. A detailed comparison reveals different orientations of A_{1A}^{-} and A_{1B}^{-} in their respective binding sites such that formation of a strong hydrogen bond from A_1^{-} to the protein backbone is possible only in the case of A_{1A}^{-}. We suggest that this is relevant to the rates of forward electron transfer from A_{1A}^{-} or A_{1B}^{-} to the iron−sulfur center F_X, which differ by a factor of 10. Thus, the present study sheds new light on the orientation of the phylloquinone acceptors in their binding pockets in PS I and the effect this has on function.

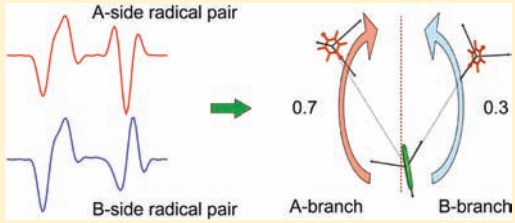

INTRODUCTION

Photosystem I (PS I) is a large macromolecular chromophore−protein supercomplex which catalyzes the light-induced oxidation of plastocyanin and reduction of ferredoxin. The majority of cofactors, which are involved in both light harvesting and light-dependent electron transfer reactions, are bound to a protein heterodimer composed of the PsaA and PsaB subunits, which in total coordinate in excess of 100 cofactors, including ∼100 chlorophyll *a* (Chl *a*), 30 *β*-carotene, and 2 phylloquinone molecules as well as 1 iron−sulfur (Fe_4S_4) cluster, denoted F_X. Two additional Fe_4S_4 clusters, called F_A and F_B, are bound by the PsaC protein subunit. Crystallographic models of PS I have been solved both in a prokaryotic system, *Synechococcus elongatus*,[1] where PS I contains only the photochemical reaction center and the proximal antennas, and in a eukaryotic system, *Pisum sativum*,[2] where PS I is composed of the reaction center and an additional light-harvesting complement. Both structures highlight a symmetrical arrangement of the electron transfer cofactors which are organized in two parallel chains relative to a pseudo-C_2 symmetry axis that is perpendicular to the membrane plane in which PS I is embedded in vivo. This structural feature is a common motif in photosynthetic reaction centers as it has been observed in all

Received: September 19, 2011
Published: February 18, 2012

 © 2012 American Chemical Society dx.doi.org/10.1021/ja208806g | *J. Am. Chem. Soc.* 2012, 134, 5563−5576

the other known crystallographic models of these pigment proteins, i.e., in the reaction centers of purple bacteria[3] and in photosystem II.[4]

Figure 1 depicts the arrangement of the electron transfer cofactors in the cyanobacterium *S. elongatus*, evaluated from an

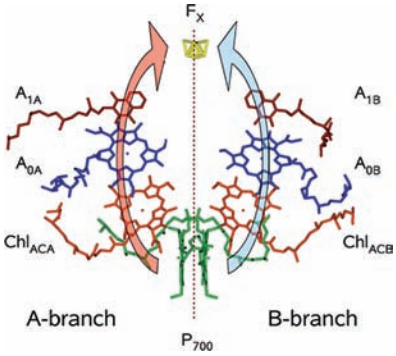

Figure 1. Arrangement of the electron transfer cofactors in photosystem I of the cyanobacterium *S. elongatus* taken from the X-ray structure at 2.5 Å resolution.[1] The figure was generated with Accelrys DS Visualizer 2.0 using the X-ray crystallographic coordinates deposited at Brookhaven data bank under accession number 1JB0, 2001. The direction of view is parallel to the membrane plane. One sees that the electron transfer cofactors are organized in two parallel branches denoted as the A- and B-branches. The dotted red line indicates the pseudo-C_2 symmetry axis perpendicular to the membrane plane. P_{700} is the ultimate electron donor comprising a chlorophyll *a*/chlorophyll *a*′ "heterodimer". Chl_{ACA} and Chl_{ACB} are the accessory chlorophylls. A_{0A} and A_{0B} are the chlorophyll acceptors. A_{1A} and A_{1B} are the phylloquinone acceptors. F_X is the first iron–sulfur cluster. The bent arrows indicate the two possible electron transfer pathways in photosystem I.

electron density map of PS I at 2.5 Å resolution.[1] The crystal structure reveals that the electron transfer chains are not completely independent but share some of the cofactors. The Chl *a*/Chl *a*′ "heterodimer", assigned to P_{700}, is coordinated at the interface of the PsaA and PsaB subunits. Similarly, the Fe_4S_4 center F_X is common to both electron transfer branches. The other cofactors, involving the accessory chlorophyll Chl_{AC}, the chlorophyll acceptor A_0, and the phylloquinone acceptor A_1, are part of either branch A or branch B.

It was initially thought that P_{700} acts as the primary electron donor in a single-step charge separation reaction. This view has been questioned by femtosecond optical studies which suggest a more complex scenario.[5,6] It was proposed that charge separation occurs between the accessory chlorophyll Chl_{AC} and the chlorophyll acceptor A_0, where Chl_{AC} acts as the primary electron donor. The primary radical pair $Chl_{AC}^{+}A_0^{-}$ is then rapidly reduced (~10 ps) by the ultimate electron donor P_{700} to form the secondary radical pair $P_{700}^{+}A_0^{-}$.[6] In about 50 ps, the electron is further transferred to the phylloquinone acceptor A_1.[6] The tertiary radical pair $P_{700}^{+}A_1^{-}$ is the first intermediate detectable by time-resolved electron paramagnetic resonance (EPR). At room temperature $P_{700}^{+}A_1^{-}$ as detected by EPR decays in about 200 ns by forward electron transfer to the Fe_4S_4 center F_X,[7,8] and mutation of residues in the PsaA phylloquinone binding pocket demonstrated that this was due to electron transfer on the PsaA branch.[9] At low temperature, the lifetime of $P_{700}^{+}A_1^{-}$ is about 150 μs, and it decays primarily by charge recombination.[10]

During the past few years a substantial body of evidence has been collected indicating that both cofactor chains in PS I are functionally relevant.[11−23] This so-called bidirectional mechanism is a characteristic of the PS I type I reaction center, as there is consistent and convincing experimental evidence that only one cofactor branch is active in the type II reaction centers of purple bacteria and in photosystem II, probably because the two quinones in these reaction centers function as a "two-electron gate". The main evidence for bidirectional electron transfer in PS I can be summarized as follows.

The room temperature oxidation of the reduced phylloquinone acceptor, A_1^{-}, as monitored by absorbance changes was found to display biphasic kinetics, characterized by lifetimes of ~20 and ~250 ns, respectively.[14,15] Mutations of residues involved in the coordination of A_{1A} increase the lifetime of the 250 ns phase, whereas analogous mutations in the binding pocket of A_{1B} increase the lifetime of the 20 ns phase.[16] These results can be rationalized in terms of a bidirectional electron transfer mechanism, in which the 250 ns phase is assigned to the oxidation of A_{1A}^{-} and the 20 ns phase is assigned to the oxidation of A_{1B}^{-}.[16] Furthermore, carotenoid pigments, acting as electrochromic markers during the slow and fast phases of A_1^{-} oxidation, indicate the involvement of both the A- and B-side phylloquinones in PS I electron transport.[17]

In addition, mutants have been studied in which specific residues, serving as the axial ligand to the primary acceptor, A_0, were exchanged in either the PsaA or PsaB subunit.[18,19] Amino acid changes in the A-side protein resulted in a decrease in the amplitude of the 250 ns phase and an increase in the amplitude of the 20 ns phase. The opposite result was observed for the B-side mutants.[18,19] Furthermore, it was found that the primary electron transfer event can be initiated independently in each branch.[6]

Further insight into the electron transfer pathways in PS I has been gained by pulsed X-band (9.5 GHz) EPR. The electron spin echo envelope modulation (ESEEM) of the spin-correlated radical pair $P_{700}^{+}A_1^{-}$ was studied in two site-directed mutants[20] in which the axial ligand to A_0 was substituted in either the PsaA or PsaB subunit. From the analysis of the ESEEM frequencies, values of the dipolar (D) and exchange (J) interactions in $P_{700}^{+}A_1^{-}$ were extracted.[21,22] The D values, observed for the site-directed mutants and the wild type, can be interpreted in terms of the two distances between P_{700}^{+} and A_1^{-}, indicating that both cofactor branches of PS I are competent in electron transfer.[21,22]

Supporting evidence for the bidirectional mechanism has been obtained from pulsed D-band (130 GHz) EPR performed on deuterated PS I preparations. Depending on the reducing conditions of the sample, two distinct radical pair spectra were observed at cryogenic temperatures.[23] Analysis revealed that the two spectra can be simulated using the same magnetic but different geometric parameters, where the latter are consistent with the cofactor arrangement of $P_{700}A_{1A}$ and $P_{700}A_{1B}$ in the X-ray structure.[23] This suggests the direct observation of two spin-correlated radical pairs in PS I arising from both the A- and B-branches of electron transfer cofactors.

There is now general agreement that both cofactor branches of PS I are competent in electron transfer. However, the molecular details of this mechanism are not yet fully understood. If electron transfer via the A- or B-branch occurs to different extents, what factors control the initial asymmetry? Why do the lifetimes of A_{1A}^{-} and A_{1B}^{-} differ by a factor of 10 despite an almost symmetric spatial arrangement of the two phylloquinones and very similar protein binding pockets? Could this difference be explained by a change in the spatial arrangements of the charge-separated states vs their "ground states"? It appears that answers to these questions cannot be

dx.doi.org/10.1021/ja208806g | J. Am. Chem. Soc. 2012, 134, 5563−5576

deduced from crystallographic models alone. The objective of the present study is to obtain spatial structures of the radical pair intermediates $P_{700}^{+}A_{1A}^{-}$ and $P_{700}^{+}A_{1B}^{-}$, independent of the crystal structure data, and thus to shed new light on the factors that influence bidirectional electron transfer in PS I. To achieve this goal, we evaluate the geometry of the tertiary radical pairs $P_{700}^{+}A_{1A}^{-}$ and $P_{700}^{+}A_{1B}^{-}$ using quantum oscillations in a two-dimensional Q-band (34 GHz) EPR experiment.[24] Previous EPR studies reveal a breaking of the approximate C_2 symmetry of the electron transfer cofactors in the electronic structure of P_{700}^{+}.[25,26] As a result, the EPR signatures of $P_{700}^{+}A_{1A}^{-}$ and $P_{700}^{+}A_{1B}^{-}$ are markedly different. Thus, we expect to observe two distinct radical pairs with different EPR geometries.

All EPR experiments are performed on deuterated wild-type cells of the green alga *Chlamydomonas reinhardtii* and the deuterated site-directed mutant PsaA-M684H of *C. reinhardtii*. Deuteration provides the greatly enhanced signal-to-noise ratio necessary for a successful detection of quantum oscillations. Furthermore, it slows the rapid decay of these oscillations due to the differences in hyperfine interactions of the radical ions. Finally, it allows for an improved orientation selection of the quantum oscillations in the two-dimensional Q-band experiment. Importantly, these experiments are performed on deuterated *whole cells* of *C. reinhardtii* at cryogenic temperatures where light-induced electron transfer is largely reversible.[21] As we employ the deuterated mutant PsaA-M684H of *C. reinhardtii*, we can exclusively detect the B-side radical pair $P_{700}^{+}A_{1B}^{-}$ by time-resolved EPR. Using deuterated wild-type cells, one can observe both radical pairs $P_{700}^{+}A_{1A}^{-}$ and $P_{700}^{+}A_{1B}^{-}$ in the transient Q-band EPR experiment.

Results are described first for the site-directed mutant PsaA-M684H[20] in which electron transfer beyond A_{0A} is impaired.[19] Analysis of the anisotropic quantum oscillations provides the orientation of the various magnetic tensors with respect to a magnetic reference frame. The orientation of the **g** tensor of P_{700}^{+} in an external reference system is adapted from a time-resolved X- and W-band (95 GHz) EPR study performed on deuterated and ^{15}N-substituted cyanobacteria.[25] Thus, we obtain the three-dimensional structure of the B-side radical pair $P_{700}^{+}A_{1B}^{-}$ following photoexcitation of PS I in its native membrane.

We then present results for deuterated wild-type cells of *C. reinhardtii* demonstrating that two different radical pairs participate in the electron transfer process. From the observed structures, these radical pairs can be assigned to $P_{700}^{+}A_{1A}^{-}$ and $P_{700}^{+}A_{1B}^{-}$. Comparison reveals different orientations of A_{1A}^{-} and A_{1B}^{-} in their respective binding sites. We suggest that this is relevant to the rates of forward electron transfer from A_{1A}^{-} or A_{1B}^{-} to the Fe_4S_4 center F_X, which differ by a factor of 10. Thus, the study of quantum oscillations, observed in a two-dimensional Q-band EPR experiment, sheds new light on the orientation of phylloquinones in their binding pockets in PS I and the function of the phylloquinone acceptors.

MATERIALS AND METHODS

Algal Strains and Culture Conditions. *C. reinhardtii* wild-type strain CC-124 was obtained from the Chlamydomonas Culture Collection at the University of Minnesota. Mutant PsaA-M684H, in which a methionine at position 684 is exchanged for histidine, was isolated at the University of London.[20] Under standard conditions the wild-type strain was grown heterotrophically in Tris−acetate−phosphate (TAP) medium[27] on agar plates (1.5% agar) or in flasks on a rotatory shaker at 23 °C under continuous irradiation with white light (photon fluence rate 45 μE m^{-2} s^{-1}) provided by fluorescent tubes (Osram L36W/25). For the mutant, which is light sensitive, only dim light (photon fluence rate 5 μE m^{-2} s^{-1}) was used.

Generation of Fully Deuterated Cells. We present here the first example of the deuteration of *C. reinhardtii*. Therefore, we provide the details of the procedures for obtaining deuterated wild-type cells of *C. reinhardtii* and the PsaA-M684H mutant. TAP medium in which 50% of the H_2O was replaced by D_2O allowed cell growth at about the same rate as in nonsupplemented TAP medium. The growth rate of the mutant strain under these conditions was retarded by a factor of about 2 as compared to that of the wild type. A stepwise adaptation to growth at higher D_2O concentrations with increments of 10% was performed on plates containing 1% agar. The plates were incubated under continuous low-intensity irradiation. For wild-type cultures adaptation to 60% D_2O took about one month. Only when cultures were fully adapted, as judged by stable generation times, was the concentration of D_2O increased. Adaptation to 70% and 80% D_2O required another month each. About nine months of continuous cultivation was needed to adapt cells to growth in TAP medium in which all H_2O had been replaced by D_2O. Once cultures were adapted to growth in 100% D_2O, deuterated acetate was used to optimize the degree of deuteration of the cells. It took about 12 months to achieve complete adaptation of the wild-type strain. For the PsaA-M684H mutant an adaptation to only 90% D_2O could be achieved. Moreover, starting from 70% D_2O, the mutant was cultivated in liquid media since it did not grow on plates at higher D_2O concentrations. Attempts to grow the deuterated PsaB-M664H mutant were unsuccessful.

Sample Preparation. For the EPR measurements, fresh cultures were grown in liquid media (D_2O) after inoculation from the plates (wild type) or the stock suspension (mutant). First, the cells were incubated without shaking for three days under continuous irradiation using a 50 mL Erlenmeyer flask with 10 mL of medium. The deuterated cells were not shaken because these cells, in contrast to cells grown in medium lacking deuterium, tended to stick to the walls of the culturing vessel at the liquid/air interface. This resulted in death of the cells. Then the cells were kept in darkness for 16 h prior to the EPR measurements. Finally, the cell suspension was transferred into a 2 mm quartz tube, irradiated at 273 K for 20 min at a wavelength of 650 nm (OPO laser, 0.8 mJ/pulse), and cooled to 100 K in the resonator of the EPR spectrometer. All samples were checked microscopically for motility and intact cell structures before the EPR experiments.

Exposure to light preferentially absorbed by photosystem II (650 nm) is known to initiate a lateral redistribution of the antenna proteins in favor of PS I.[28] Within a few minutes, an extensive supramolecular reorganization converts the photosynthetic apparatus of *C. reinhardtii* from a carbon fixation device (linear electron flow) to an adenosine triphosphate generator (cyclic electron flow).[28] It was found that this so-called "state transition" is associated with a significant increase in the radical pair signal in both the deuterated wild-type cells and the deuterated PsaA-M684H mutant of *C. reinhardtii*.

Q-Band EPR Measurements. The time-resolved Q-band EPR experiments were carried out using a transient Q-band bridge (Bruker ER050QGT) in combination with a Bruker ESP300E console. Home-made software was used to set the magnetic field under the control of an NMR teslameter (Bruker ER035M). The magnetic field was calibrated against Li:LiF (Institute of Crystallography, Moscow), which is a good standard for low-temperature measurements.[29] Irradiation of the sample was performed in a cylindrical cavity with a loaded Q of approximately 700. This corresponds to a bandwidth of 50 MHz. A frequency counter (Hewlett-Packard HP535B) was used to monitor the microwave frequency in the Q-band range. The temperature of the samples was controlled using a helium flow cryostat (Oxford CF-935). All measurements were performed at 100 K. To avoid magneto-orientation effects,[30] the samples were cooled in the absence of a magnetic field.

Optical excitation was carried out with an OPO system (OPTA GmbH) pumped by a Nd:YAG laser (Spectra Physics Quanta Ray GCR 190-10) at a wavelength of 670 nm and with a pulse width of 2.5 ns. For the actual experiment, the intensity was attenuated to 2 mJ/pulse. The repetition rate of the laser was 10 Hz. A transient recorder

dx.doi.org/10.1021/ja208806g | J. Am. Chem. Soc. 2012, 134, 5563−5576

(LeCroy 935A) was used to digitize the signal with a time resolution of 2 ns at 11 bit precision. Typically, 1000−2000 transients were accumulated to improve the signal/noise ratio. A weak laser-induced cavity signal was eliminated by subtracting transients accumulated at off-resonance conditions. A chlorophyll triplet signal, superimposed on the radical pair signal, was subtracted using a linear interpolation procedure.

Computations. A Fortran program package was used to analyze the time-resolved EPR experiments.[31] The programs calculate EPR time profiles and transient spectra of spin-correlated radical pairs with a spatially fixed geometry. The structural parameters were evaluated using a nonlinear least-squares fit procedure based on the Levenberg−Marquardt algorithm.[32] Parallel execution was utilized for the powder averaging procedure.

THEORY

In this section we briefly summarize a quantum mechanical model used in the analysis of transient Q-band EPR experiments on the radical pair intermediates $P_{700}^{+}A_1^{-}$. Particular emphasis is given to quantum oscillations detectable at early times after pulsed laser excitation.[33−40] The quantum beats are highly sensitive probes for the geometry of the charge-separated state.[24]

Spin Hamiltonian. The spin Hamiltonian employed, H, considers Zeeman, dipolar, exchange, and hyperfine interactions of the radical pair. Thus, H can be written as

$$H = \beta \mathbf{B}_0 \cdot (\mathbf{g}_1 \cdot \mathbf{S}_1 + \mathbf{g}_2 \cdot \mathbf{S}_2) + 2\mathbf{S}_1 \cdot \mathbf{D} \cdot \mathbf{S}_2 - 2J\mathbf{S}_1 \cdot \mathbf{S}_2 + \sum_k \mathbf{S}_1 \cdot \mathbf{A}_{1k} \cdot \mathbf{I}_{1k} + \sum_l \mathbf{S}_2 \cdot \mathbf{A}_{2l} \cdot \mathbf{I}_{2l} \quad (1)$$

where β, $\mathbf{B}_0$, $\mathbf{g}_i$, $\mathbf{S}_i$, $\mathbf{D}$, J, $\mathbf{A}_{ij}$ and $\mathbf{I}_{ij}$ are the Bohr magneton, the external magnetic field, the $\mathbf{g}$ tensor of radical i, the electron spin operator of radical i, the dipolar coupling tensor, the strength of the isotropic exchange interaction, the hyperfine coupling tensor between nucleus j and radical i, and the nuclear spin operator of nucleus j in site i, respectively. In the presence of a microwave field, a microwave term must be added to the spin Hamiltonian of eq 1. Note that *pseudosecular terms of the electron spin−spin interactions* are explicitly considered in the analysis. These terms are essential for the modeling of quantum oscillations and thus provide the basis for the present study.

Formation of Quantum Oscillations. The crucial point is the specification of the initial condition of $P_{700}^{+}A_1^{-}$ at the instant of the laser pulse. In wild-type cells of *C. reinhardtii*, the lifetime of the secondary radical pair $P_{700}^{+}A_0^{-}$ is short, i.e., approximately 50 ps. Thus, even the tertiary radical pairs $P_{700}^{+}A_{1A}^{-}$ and $P_{700}^{+}A_{1B}^{-}$ are generated in a virtually pure singlet state, determined by the spin multiplicity of the excited primary donor. Generally, such singlet radical pairs are formed with spin-correlated population of only half of the eigenstates[41−43] and with zero quantum electron[33−40] and single quantum nuclear[40] coherences between these states. Analysis reveals that in Q-band studies only electron spin oscillations can be observed.[40]

The formation of the quantum oscillations can be rationalized in terms of the nonadiabatic change of the spin Hamiltonian at the instant of the laser pulse. At time zero, the radical pair is created in a singlet state as a consequence of spin conservation in an ultrafast photochemical reaction. Since the singlet is not an eigenstate of the corresponding spin Hamiltonian, the radical pair starts out in a coherent superposition of eigenstates, which manifests itself as quantum oscillations in an EPR experiment with adequate time resolution.

Neglecting all anisotropic hyperfine interactions, the (rotating frame) spin Hamiltonian of the radical pair can be diagonalized analytically for any number of hyperfine coupled nuclei in the donor and acceptor radical ions. Under these conditions, the model predicts the formation of electron spin oscillations whose frequency ω_{ZQ} sensitively depends on the orientation Ω of the radical pair in the laboratory frame, $\mathbf{x}$, $\mathbf{y}$, $\mathbf{z}$, with $\mathbf{B}_0$ along the z axis. Generally, $\omega_{ZQ}(\Omega)$ can be written as[24,25,37,38]

$$\omega_{ZQ}(\Omega) = (1/\hbar)\left\{\left[\frac{2}{3}D^{zz}(\Omega) - 2J\right]^2 + [(g_1^{zz}(\Omega) - g_2^{zz}(\Omega))\beta B_0 + \sum_k a_{1k}M_{1k}^i - \sum_l a_{2l}M_{2l}^j]^2\right\}^{1/2}$$
$$M_{1k}^i = I_{1k}, I_{1k} - 1, ..., -I_{1k}$$
$$M_{2l}^j = I_{2l}, I_{2l} - 1, ..., -I_{2l} \quad (2)$$

where $D^{zz}(\Omega)$, $g_i^{zz}(\Omega)$, and a_{ij} are the zz component of the dipolar coupling tensor, the zz component of the $\mathbf{g}$ tensor of radical i, and the isotropic hyperfine coupling between nucleus j and radical i. Inspection of eq 2 reveals that the frequency of the electron spin oscillations is determined by the spin−spin interactions of the radical pair and the difference in the Zeeman and hyperfine interactions of the constituent radicals. For the tertiary radical pair of PS I, $P_{700}^{+}A_1^{-}$, the Zeeman term provides the largest contribution even in X-band EPR experiments.

In deriving eq 2, all anisotropic hyperfine interactions have been ignored. As a result, light-induced nuclear spin oscillations[40,44,45] are neglected. The latter is certainly a good approximation for Q-band studies, since the modulation amplitude of these coherences decreases strongly with the applied magnetic field. For the analysis of X-band experiments, however, consideration of anisotropic hyperfine interactions is essential.

Radical Pair Geometry. The orientation dependence of the magnetic tensor elements $g_i^{zz}(\Omega)$ and $D^{zz}(\Omega)$ can be evaluated by a 2-fold transformation. In the first step, we transform from the principal axis system $\mathbf{X}_i$, $\mathbf{Y}_i$, $\mathbf{Z}_i$ of the respective magnetic tensor to a magnetic reference system, $\mathbf{X}$, $\mathbf{Y}$, $\mathbf{Z}$, using the Euler angles[46] $\Omega_i = (\Phi_i, \Theta_i, \Psi_i)$ (see Figure 2). For convenience, this reference system is chosen parallel to the principal axis system of the $\mathbf{g}$ tensor of A_1^{-}. In the second step, we transform by the Euler angles[46] $\Omega = (\Phi, \Theta, 0)$ into the laboratory frame $\mathbf{x}$, $\mathbf{y}$, $\mathbf{z}$ (see Figure 2). A random distribution of the radical pair with respect to the laboratory frame is considered by averaging over Φ and Θ.

In our model, the orientation of the magnetic tensors ($\mathbf{g}$ tensor of P_{700}^{+}, dipolar tensor) with respect to the magnetic reference system ($\mathbf{g}$ tensor of A_1^{-}) is described by the five Euler angles Φ_1, Θ_1, Ψ_1, Θ_D, and Ψ_D. They constitute the geometry of the radical pair. Values for these angles are extracted from a two-dimensional Q-band EPR experiment using the pronounced variation of the quantum oscillations across the powder spectrum.[24,25,47−53]

Two-dimensional Correlation Spectroscopy. Our strategy to obtain the geometry of the radical pair involves transient nutation experiments performed at Q-band frequencies. In these experiments, the sample is irradiated with a short laser pulse and the time evolution of the transverse magnetization is

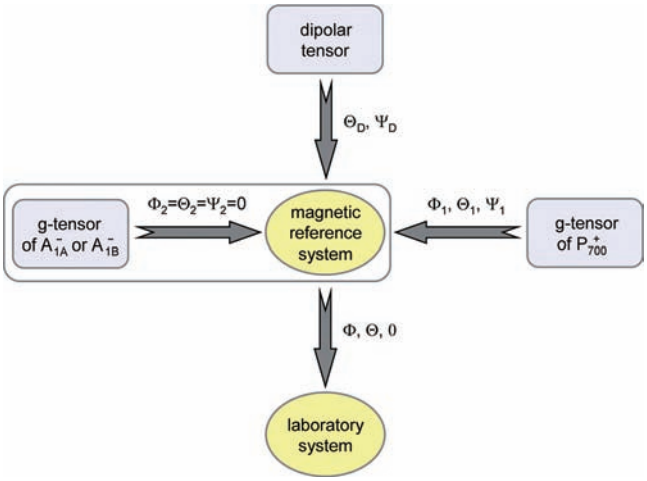

Figure 2. Notation for magnetic tensor systems and Euler transformations used in the EPR model. P_{700}^+ is the oxidized ultimate electron donor. A_{1A}^- and A_{1B}^- are the reduced phylloquinone acceptors. The orientation dependence of the magnetic tensor elements is evaluated by a 2-fold transformation. In the first step, we transform from the principal axis system $\mathbf{X}_i$, $\mathbf{Y}_i$, $\mathbf{Z}_i$ of the respective magnetic tensor to a magnetic reference system, **X**, **Y**, **Z**. For convenience, the magnetic reference system is chosen parallel to the **g** tensor of A_{1A}^- or A_{1B}^-. In the second step, we transform from **X**, **Y**, **Z** to the laboratory frame **x**, **y**, **z**. In our model, the orientation of the magnetic tensors (**g** tensor of P_{700}^+, dipolar tensor) with respect to the magnetic reference system is described by the five Euler angles Φ_1, Θ_1, Ψ_1, Θ_D, and Ψ_D. They constitute the geometry of the radical pair.

detected in the presence of a weak microwave magnetic field. Generally, about 80 different time profiles are taken at equidistant field points covering the total spectral width. This yields a two-dimensional data set in which the zero quantum and the single quantum electron coherences of the radical pair are correlated with each other. A computer fit of the two-dimensional correlation experiment provides values for *all five Euler angles* of the radical pair geometry. The convergence of the fit was checked using a calculated data set. The fit was repeated multiple times with different starting values covering the parameter space. The *correct* global minimum values were found in about 25% of all runs. In the remaining fits local side minima were reached.

RESULTS

Geometry of the B-Side Radical Pair. To determine the geometry of $P_{700}^+A_{1B}^-$, we use two-dimensional nutation EPR experiments performed at Q-band frequencies. Generally, a complete data set consists of transient signals taken at equidistant field points covering the total spectral width. This yields a two-dimensional variation of the signal intensity with respect to both the magnetic field and the time axis. Transient spectra can be extracted from such a plot at any fixed time after the laser pulse as slices parallel to the magnetic field axis. Likewise, the time evolution of the transverse magnetization may be obtained for any given field as a slice along the time axis.

Typical Q-band EPR spectra, extracted from the two-dimensional data set of the deuterated PsaA-M684H mutant, are shown in Figure 3 (solid red lines). The spectra refer to four different times after the laser pulse, a microwave frequency of $\omega/2\pi$ = 34.100 GHz, a microwave field of B_1 = 0.085 mT, and T = 100 K. Note that a positive signal indicates absorptive (a)

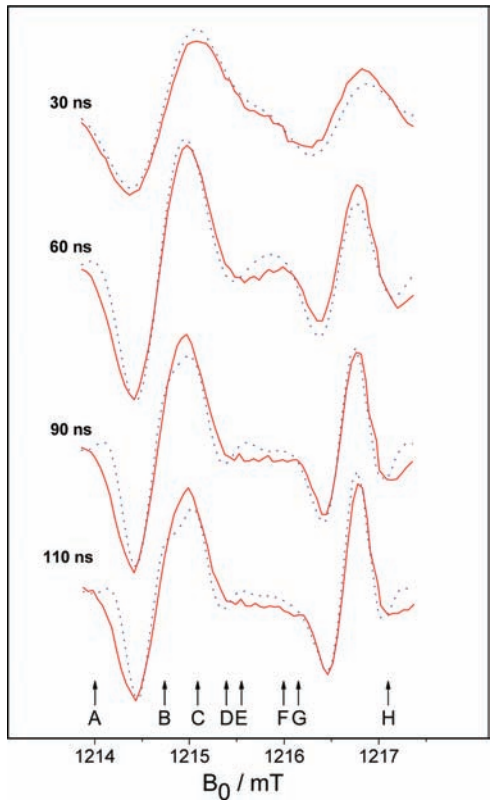

Figure 3. Transient Q-band EPR spectra of the light-induced radical pair $P_{700}^+A_{1B}^-$ in photosystem I at various times after the laser pulse. Positive signals indicate absorptive and negative signals emissive spin polarization. The microwave frequency $\omega/2\pi$ = 34.100 GHz, and the microwave field B_1 = 0.085 mT. Full red lines: experimental spectra from the deuterated PsaA-M684H mutant of *C. reinhardtii*. The temperature T = 100 K. Dotted blue lines: calculated spectra using the Euler angles given in Table 1. Various field positions are marked from A to H. The time evolution of the transverse magnetization at these field positions is shown in Figure 4.

and a negative signal emissive (e) spin polarization. Evidently, the early spectrum is much broader than the later ones. Moreover, the polarization changes from a simple e/a/e/a pattern at early times to a characteristic e/a/e/a/e pattern at later times.

Figure 4 depicts the short time behavior of the transverse magnetization (solid red lines) measured at eight selected field positions (A–H, Figure 3). Evidently, there are fast initial oscillations which disappear 100 ns after the laser pulse. Basically, these oscillations represent quantum beats, associated with the spin-correlated generation of the radical pair (s).[33−40]Note that the amplitude and frequency of the quantum beats vary significantly across the powder spectrum. This pronounced variation can be used to evaluate the mutual orientation of the magnetic tensors in the radical pair(s).

In previous pulsed low-temperature EPR studies of the nondeuterated PsaA-M684H mutant of *C. reinhardtii*, the out-of-phase electron spin echo was found to decay with a single exponential.[20,21] The observed decay constant is indicative of B-branch electron transfer. This together with the analysis of the ESEEM frequencies[21] indicates that only the B-side radical pair can be detected under these conditions. We adopt this result in the analysis of the two-dimensional Q-band experiment performed on the deuterated mutant.

dx.doi.org/10.1021/ja208806g | *J. Am. Chem. Soc.* 2012, 134, 5563−5576

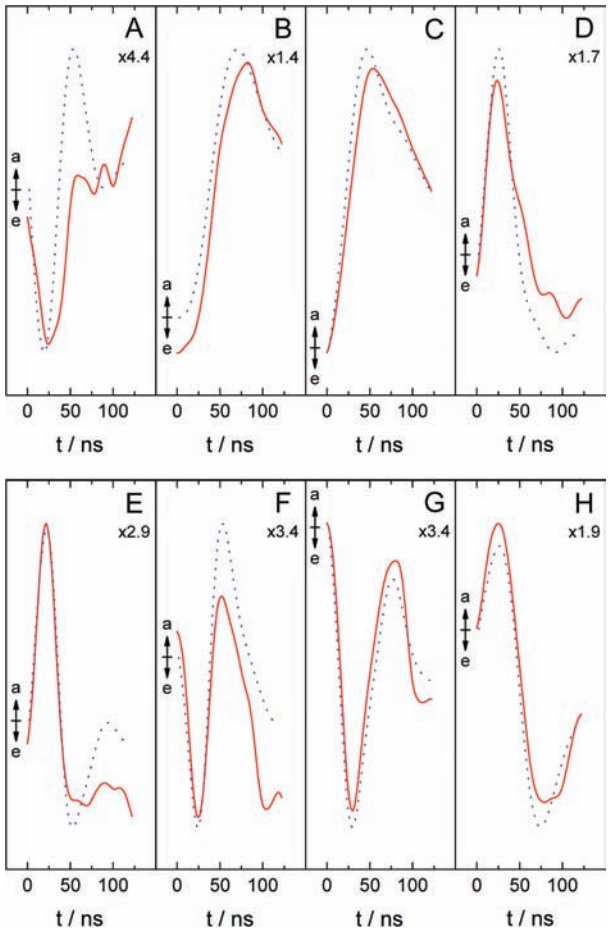

Figure 4. Time evolution of the transverse Q-band magnetization of the light-induced radical pair $P_{700}^{+}A_{1B}^{-}$ in photosystem I immediately after the laser pulse. The transients refer to eight different static magnetic fields (positions A–H, Figure 3). Positive and negative signals indicate absorptive and emissive polarizations, respectively. The microwave frequency $\omega/2\pi$ = 34.100 GHz, and the microwave field B_1 = 0.085 mT. Full red lines: experimental time profiles from the deuterated PsaA-M684H mutant of *C. reinhardtii*. The temperature T = 100 K. Dotted blue lines: calculated time profiles using the Euler angles given in Table 1.

The fixed magnetic parameters, underlying this analysis, are available from independent EPR experiments (see the Supporting Information, Table S1). The **g** tensor components of P_{700}^{+} and A_1^{-} were adapted from previous high-field EPR studies of various PS I preparations.[54−56] The spin−spin coupling parameters of $P_{700}^{+}A_{1B}^{-}$, D_B and J_B, have been determined by an ESEEM study of $P_{700}^{+}A_{1B}^{-}$ in the non-deuterated PsaA-M684H mutant.[21] Hyperfine interactions in the radical pair were approximated by considering five equivalent ^{14}N nuclei (a_N = 0.060 mT) in P_{700}^{+} and four equivalent ^{2}H nuclei (a_D = 0.055 mT) in A_1^{-}. The resultant second moments are in agreement with published hyperfine parameters for P_{700}^{+} [57,58] and A_1^{-}.[59,60] Inhomogeneous broadening was considered by convolution with a Gaussian. The homogeneous spin−spin relaxation time has been estimated from the decay of the out-of-phase electron spin echo of $P_{700}^{+}A_{1B}^{-}$ in the nondeuterated PsaA-M684H mutant.[21]

The orientation of the magnetic tensors of $P_{700}^{+}A_{1B}^{-}$ (**g** tensor of P_{700}^{+}, dipolar tensor) with respect to the magnetic reference system (**g** tensor of A_{1B}^{-}) can be described by the five Euler angles Φ_{1B}, Θ_{1B}, Ψ_{1B}, Θ_{DB}, and Ψ_{DB}. Values for these angles were obtained from a computer fit of the two-dimensional Q-band experiment using the pronounced variation of the quantum oscillations across the powder spectrum. Notably, the full spectral width of 3.4 mT and a time range of 120 ns were considered. Thus, 69 calculated time profiles, involving 4209 data points, were simultaneously fitted to the experimental profiles by varying the Euler angles of the radical pair geometry. In the calculations, the limited resonator bandwidth of 30 MHz was taken into account by using a Gaussian response function. Finally, spin relaxation was considered by multiplying each time profile by an exponential decay curve, characterized by the transverse relaxation time T_2 (see the Supporting Information, Table S1).

The fit was repeated multiple times with different starting values covering the parameter space. The same global minimum values were found in 22% of all runs. In the remaining fits local side minima were reached. In Figures 3 and 4 we compare experimental line shapes and time profiles (solid red lines) with the best simulation (dotted blue lines) based on the angular values (see Table 1, columns 1−3)

Table 1. Euler Angles Characterizing the Orientation of the Magnetic Tensors of the B-Side Radical Pair $P_{700}^{+}A_{1B}^{-}$ in Photosystem I

orientation of the magnetic tensors in $P_{700}^{+}A_{1B}^{-}$ [a]			orientation of the **g** tensor of P_{700}^{+} [b]	
notation[c]	angular value (deg)	systematic error[d] (deg)	notation[e]	angular value (deg)
Φ_{1B}	32	±4	Φ_1^{Chl}	183
Θ_{1B}	124	±14	Θ_1^{Chl}	29
Ψ_{1B}	132	±3	Ψ_1^{Chl}	220
Θ_{DB}	70	±3		
Ψ_{DB}	23	±3		

[a]Evaluated in this study using the deuterated PsaA-M684H mutant of *C. reinhardtii*. [b]Determined by high-time-resolution X- and W-band EPR using deuterated and ^{15}N-substituted cyanobacteria (see the Supporting Information).[25] [c]The Euler angles Φ_{1B}, Θ_{1B}, Ψ_{1B}, Θ_{DB}, and Ψ_{DB} transform from the principal axis system of the respective tensor (**g** tensor of P_{700}^{+}, dipolar tensor) to the magnetic reference system (**g** tensor of A_{1B}^{-}). [d]The cited errors consider the uncertainties in the published **g** tensor components.[52] [e]The Euler angles Φ_1^{Chl}, Θ_1^{Chl}, and Ψ_1^{Chl} transform from the principal axis system of the **g** tensor of P_{700}^{+} to the chlorophyll-based reference system $\mathbf{X}^{Chl}$, $\mathbf{Y}^{Chl}$, $\mathbf{Z}^{Chl}$. The Z^{Chl} axis is the chlorophyll normal; the Y^{Chl} axis is the projection of the membrane normal onto the chlorophyll plane. The X^{Chl} axis then lies in the chlorophyll plane perpendicular to $\mathbf{Y}^{Chl}$.

$$\Phi_{1B} = 32° \pm 4°,$$
$$\Theta_{1B} = 124° \pm 14°,$$
$$\Psi_{1B} = 132° \pm 3°,$$
$$\Theta_{DB} = 70° \pm 3°,$$
$$\Psi_{DB} = 23° \pm 3°$$

The agreement achieved is good in view of the degree of deuteration of only 90% obtained for the PsaA-M684H mutant. The cited errors are systematic errors, which consider the uncertainties in the published **g** tensor components.[52]

It should be noted that the fit of the two-dimensional Q-band experiment does not provide a unique set of Euler angles for

dx.doi.org/10.1021/ja208806g | *J. Am. Chem. Soc.* 2012, 134, 5563−5576

the geometry of the B-side radical pair. This ambiguity is a general problem in the analysis of magnetic resonance experiments since these techniques cannot in general distinguish between a positive and a negative magnetic tensor orientation. In fact, the two **g** tensors exhibit D_{2h} symmetry and are therefore invariant under 180° rotations about their principal axes. The axially symmetric dipolar tensor transforms according to the point group $D_{\infty h}$. Consequently, it is invariant under 180° rotation about any axis perpendicular to the symmetry axis. Applying these magnetic tensor rotations, 32 equivalent radical pair geometries are obtained (see the Supporting Information, Table S2).[24,52] They can be divided into eight groups with four geometries where the latter yield indistinguishable spatial structures. Thus, only an 8-fold degeneracy of the radical pair geometry actually exists. For studies of the radical pair spectra, this degeneracy is not critical since all eight representations yield the same spin-polarized EPR spectrum.

In structural studies, however, the degeneracy of the geometry has to be eliminated. This can be achieved by a critical evaluation of the radical pair structures calculated from the various Q-band geometries and the known orientation of one **g** tensor in an external reference system. The crucial parameter is the position of A_{1A}^- (A_{1B}^-) in the photosynthetic membrane.[24,52] We assume that a shift of A_{1A}^- (A_{1B}^-) relative to the position of A_{1A} (A_{1B}) in the X-ray structure beyond the error limits of the Q-band study is unlikely to occur.[61] Using the quinone position as a selection criterion, one can eliminate seven of the eight degenerate geometries. Thus, a *unique* radical pair structure is obtained.

Geometry of the A-Side Radical Pair. To evaluate the geometry of $P_{700}^+A_{1A}^-$, we extend the EPR studies to the wild-type cells, where it has been shown that both cofactor branches are competent.[6,14−23] Typical Q-band EPR spectra of $P_{700}^+A_1^-$, observed 30, 60, 90, and 110 ns after the laser pulse, are depicted in Figure 5 (solid red lines). The spectra refer to deuterated wild-type cells of *C. reinhardtii*, a microwave frequency of $\omega/2\pi$ = 34.090 GHz, a microwave field of B_1 = 0.050 mT, and T = 100 K. One sees that the early spectrum is much broader than the later ones, which we attribute to lifetime broadening.[62] Moreover, the spectral shape changes significantly with time. The characteristic e/a/a/e/a pattern, observed at later times, is in agreement with results found for deuterated cyanobacteria under comparable experimental conditions.[25,26]

In Figure 6 we compare transient Q-band EPR spectra of $P_{700}^+A_1^-$, observed in the deuterated wild-type cells (Figure 6a) and the deuterated PsaA-M684H mutant (Figure 6b) of *C. reinhardtii*. Each of the two EPR spectra was extracted 110 ns after the laser pulse from the corresponding two-dimensional data set. Comparison reveals that the line shapes of the low-field portions of the radical pair spectra are similar, but the high-field parts are markedly different. In fact, the observed polarization pattern changes from e/a/a/e/a in the case of the wild-type cells to e/a/e/a/e for the PsaA-M684H mutant. This is clear evidence for a change in the relative orientations of the two constituents of the radical pair giving rise to the spectrum and thus a major change in the electron transfer pathway within PS I.

Figure 7 depicts the short time behavior of the transverse magnetization (solid red lines), observed for the deuterated wild-type cells of *C. reinhardtii*. The time profiles refer to eight selected field positions (A−H) as indicated in Figure 5. Evidently, there are quantum oscillations which disappear 100 ns

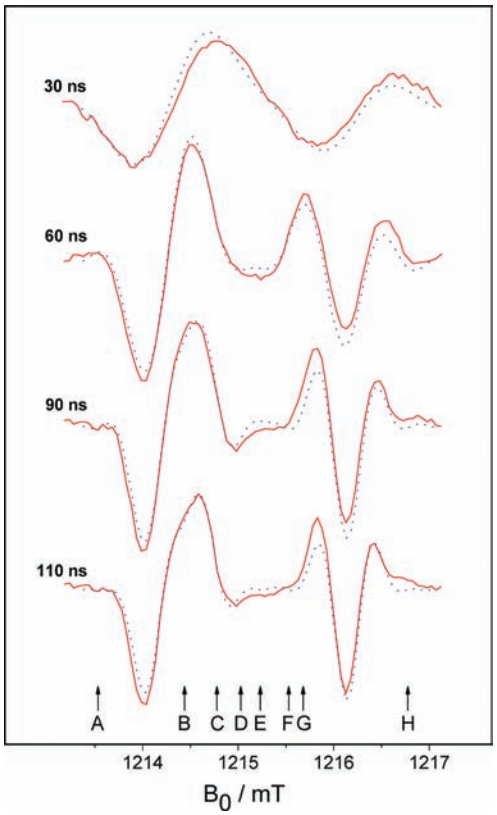

Figure 5. Transient Q-band EPR spectra of the light-induced radical pairs $P_{700}^+A_{1A}^-$ and $P_{700}^+A_{1B}^-$ in photosystem I at various times after the laser pulse. Positive signals indicate absorptive and negative signals emissive spin polarization. The microwave frequency $\omega/2\pi$ = 34.090 GHz, and the microwave field B_1 = 0.050 mT. Full red lines: experimental spectra from deuterated wild-type cells of *C. reinhardtii*. The temperature T = 100 K. Dotted blue lines: calculated spectra using a mole fraction of x_A = 0.71 for the A-side radical pair and the Euler angles given in Tables 1 and 2. Various field positions are marked from A to H. The time evolution of the transverse magnetization at these field positions is shown in Figure 7.

after the laser pulse. Generally, oscillation frequencies from 10 to 50 MHz can be extracted from the corresponding power spectra. Note that the amplitude and the frequency of the quantum beats vary significantly across the powder spectrum. This pronounced variation can be used to evaluate the geometry of the radical pair(s) involved in the electron transfer process.

In a pulsed low-temperature EPR study of nondeuterated wild-type cells of *C. reinhardtii*, the out-of-phase electron spin echo of $P_{700}^+A_1^-$ was found to decay with two exponentials.[20,21] This together with ESEEM analysis[21] suggests that both radical pairs $P_{700}^+A_{1A}^-$ and $P_{700}^+A_{1B}^-$ can be detected under these conditions. The fixed magnetic parameters, used in the computer fit of the two-dimensional EPR experiment, are summarized elsewhere (see the Supporting Information, Table S1). The **g** tensor components[54−56] and the parameters of the hyperfine interaction[57−60] are the same as those employed in the case of the deuterated mutant. However, as we consider both radical pair intermediates $P_{700}^+A_{1A}^-$ and $P_{700}^+A_{1B}^-$, two sets of spin−spin coupling parameters, D_A, J_A and D_B, J_B, are now required in the analysis.[21]

For convenience, the geometry of $P_{700}^+A_{1B}^-$ was adopted from the mutant study (see the preceding section). The mole

dx.doi.org/10.1021/ja208806g | J. Am. Chem. Soc. 2012, 134, 5563−5576

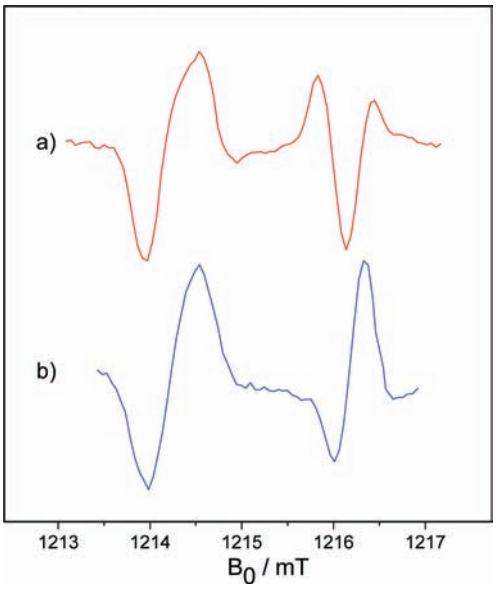

Figure 6. Comparison of experimental Q-band EPR spectra of the radical pairs $P_{700}^{+}A_{1A}^{-}$ and $P_{700}^{+}A_{1B}^{-}$ in photosystem I. Positive signals indicate absorptive and negative signals emissive spin polarization. Each of the two transient EPR spectra was extracted 110 ns after the laser pulse from a two-dimensional data set. The microwave frequency $\omega/2\pi$ = 34.090 GHz, and the temperature T = 100 K. (a) Experimental EPR spectrum from deuterated wild-type cells of *C. reinhardtii*. The microwave field B_1 = 0.050 mT. (b) Experimental EPR spectrum from the deuterated PsaA-M684H mutant of *C. reinhardtii*. The microwave field B_1 = 0.085 mT.

fraction of $P_{700}^{+}A_{1A}^{-}$, x_A, and the orientation of the magnetic tensors in $P_{700}^{+}A_{1A}^{-}$ were obtained from a computer fit of the two-dimensional Q-band experiment on the wild-type cells. Notably, a spectral width of 3.7 mT and a time range of 130 ns were considered. Thus, 79 calculated time profiles involving 4950 data points were simultaneously fitted to the experimental profiles by varying the geometry parameters and the mole fraction of $P_{700}^{+}A_{1A}^{-}$. In the calculations, the limited resonator bandwidth of 50 MHz was taken into account by using a Gaussian response function. Finally, spin relaxation was considered by multiplying each time profile by an exponential decay curve, characterized by the transverse relaxation time T_2 (see the Supporting Information, Table S1).

The fit was repeated multiple times with different starting values covering the parameter space. The same global minimum values were found in about 22% of all runs. In the remaining fits local side minima were reached. In Figures 5 and 7 we compare experimental line shapes and time profiles (solid red lines) with the best fit simulation (dotted blue lines) based on the parameter values (see Table 2, columns 1−3)

$$x_A = 0.71 \pm 0.02$$

$$\Phi_{1A} = 226° \pm 4°,$$

$$\Theta_{1A} = 88° \pm 13°,$$

$$\Psi_{1A} = 319° \pm 3°,$$

$$\Theta_{DA} = 71° \pm 3°,$$

$$\Psi_{DA} = 11° \pm 6°$$

Generally, the agreement achieved is good. The cited errors are systematic errors, evaluated as described previously.[52]

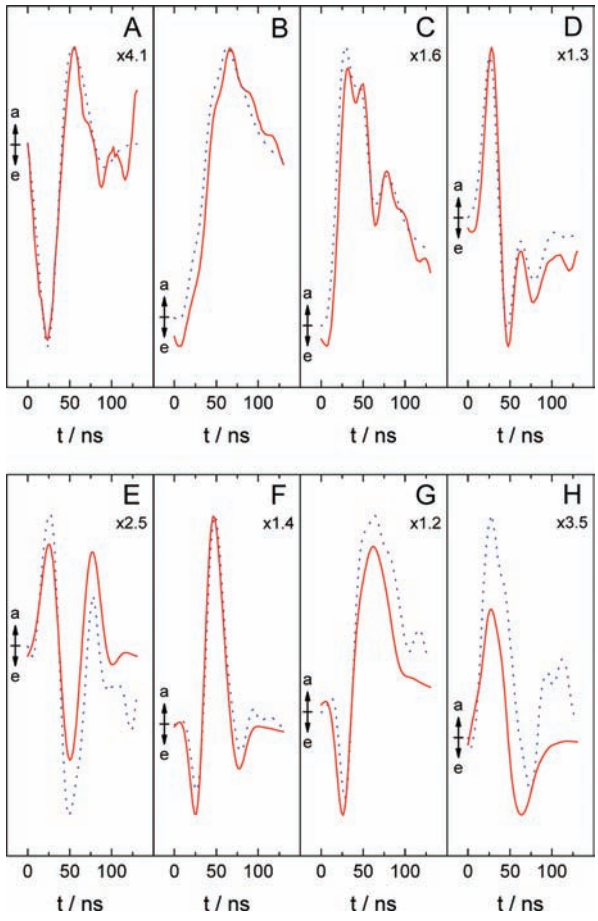

Figure 7. Time evolution of the transverse Q-band magnetization of the light-induced radical pairs $P_{700}^{+}A_{1A}^{-}$ and $P_{700}^{+}A_{1B}^{-}$ in photosystem I immediately after the laser pulse. The transients refer to eight different static magnetic fields (positions A−H, Figure 5). Positive and negative signals indicate absorptive and emissive polarizations, respectively. The microwave frequency $\omega/2\pi$ = 34.090 GHz, and the microwave field B_1 = 0.050 mT. Full red lines: experimental time profiles from deuterated wild-type cells of *C. reinhardtii*. The temperature T = 100 K. Dotted blue lines: calculated time profiles using a mole fraction of x_A = 0.71 for the A-side radical pair and the Euler angles given in Tables 1 and 2.

Analysis reveals that in the wild-type cells of *C. reinhardtii* both cofactor branches are functionally relevant. From the mole fractions of the two radical pairs, x_A = 0.71 and x_B = 0.29, evaluated at cryogenic temperatures, an "effective branching ratio" (B/A) of 0.41 is deduced. It should be emphasized that normally the term branching ratio refers to the extent to which electrons pass along either the A- or B-branch of electron transfer in PS I following excitation by light at room temperature. In optical spectroscopy, this ratio is determined by a global analysis of transient absorption hypersurfaces which provide the lifetimes and transient populations of all six radical pair states involved in the bidirectional electron transfer. Here we are measuring an effective branching ratio at cryogenic temperatures by looking at the relative proportions to which electrons excited by a flash of light reside in either of the light-induced radical pairs $P_{700}^{+}A_{1A}^{-}$ and $P_{700}^{+}A_{1B}^{-}$.

Room temperature studies of *C. reinhardtii* using transient absorption and transient EPR spectroscopy[6,18] have reported B/A branching ratios of 0.61 and 0.67. These are higher than the effective B/A branching ratio of 0.41 we have determined at cryogenic temperatures. We believe this difference can be

Table 2. Euler Angles Characterizing the Orientation of the Magnetic Tensors of the A-Side Radical Pair $P_{700}^{+}A_{1A}^{-}$ in Photosystem I

orientation of the magnetic tensors in $P_{700}^{+}A_{1A}^{-}$ [a]			orientation of the **g** tensor of P_{700}^{+} [b]	
notation[c]	angular value (deg)	systematic error[d] (deg)	notation[e]	angular value (deg)
Φ_{1A}	226	±4	Φ_1^{Chl}	183
Θ_{1A}	88	±13	Θ_1^{Chl}	29
Ψ_{1A}	319	±3	Ψ_1^{Chl}	220
Θ_{DA}	71	±3		
Ψ_{DA}	11	±6		

[a]Evaluated in this study using deuterated wild-type cells of *C. reinhardtii*. [b]Determined by high-time-resolution X- and W-band EPR using deuterated and ^{15}N-substituted cyanobacteria (see the Supporting Information).[25] [c]The Euler angles Φ_{1A}, Θ_{1A}, Ψ_{1A}, Θ_{DA}, and Ψ_{DA} transform from the principal axis system of the respective tensor (**g** tensor of P_{700}^{+}, dipolar tensor) to the magnetic reference system (**g** tensor of A_{1A}^{-}). [d]The cited errors consider the uncertainties in the published **g** tensor components.[52] [e]The Euler angles Φ_1^{Chl}, Θ_1^{Chl}, and Ψ_1^{Chl} transform from the principal axis system of the **g** tensor of P_{700}^{+} to the chlorophyll-based reference system $\mathbf{X}^{Chl}$, $\mathbf{Y}^{Chl}$, $\mathbf{Z}^{Chl}$. The Z^{Chl} axis is the chlorophyll normal. The Y^{Chl} axis is the projection of the membrane normal onto the chlorophyll plane. The X^{Chl} axis then lies in the chlorophyll plane perpendicular to $\mathbf{Y}^{Chl}$.

rationalized in terms of a bidirectional kinetic model[11] considering the different temperatures at which the branching ratios were determined and the blocking of forward electron transfer from A_{1B}^{-} to F_X at cryogenic temperatures (see the Supporting Information), although the possibility of equilibration between the two phylloquinones via F_X at room temperature[63] further complicates comparisons between optical and EPR measurements carried out at room and cryogenic temperatures.

Spatial Structure of the A-Side Radical Pair. To determine the spatial structure of the A-side radical pair, knowledge of the orientation of one **g** tensor of $P_{700}^{+}A_{1A}^{-}$ in an external reference system is required. This information exists for P_{700}^{+}, where the **g** tensor was determined by high-time-resolution X- and W-band EPR using deuterated and ^{15}N-substituted cyanobacteria.[25] To describe the **g** tensor orientation of P_{700}^{+}in the A-side radical pair, we define a chlorophyll-based reference system, $\mathbf{X}^{Chl}$, $\mathbf{Y}^{Chl}$, $\mathbf{Z}^{Chl}$, which corresponds to the reference system used for the primary donor in purple bacteria.[64] The Z^{Chl} axis is the chlorophyll normal; the Y^{Chl} axis is the projection of the membrane normal onto the chlorophyll plane. The X^{Chl} axis then lies in the chlorophyll plane perpendicular to $\mathbf{Y}^{Chl}$. In this reference system, the orientation of the **g** tensor of P_{700}^{+} in $P_{700}^{+}A_{1A}^{-}$ can be described by four sets of Euler angles, denoted by orientations I, II, III, and IV (see the Supporting Information, Table S3).

The structural ambiguity can be eliminated by a critical evaluation of the radical pair structures of $P_{700}^{+}A_{1A}^{-}$ calculated from the eight degenerate Q-band geometries and the four possible **g** tensor orientations. The crucial parameter is the position of A_{1A}^{-} in the photosynthetic membrane. For **g** tensor orientation I (see Table 2, columns 4 and 5)

$$\Phi_1^{Chl} = 183°,\ \Theta_1^{Chl} = 29°,\ \Psi_1^{Chl} = 220°$$

A_{1A}^{-} is shifted by 2.5 Å from the position determined by X-ray crystallography. This shift appears to be insignificant in view of the uncertainty of ±5.5 Å, estimated from the systematic errors of the Q-band study.[61] Use of **g** tensor orientation II leads to a quinone shift which is beyond the EPR error limits. Consequently, **g** tensor orientation II is eliminated. Similarly, **g** tensor orientations III and IV can be ignored since they lead to A_{1A}^{-} positions which are incompatible with the X-ray structure. We therefore conclude that **g** tensor orientation I is correct. This conclusion confirms the previous assignment in time-resolved high-frequency and multifrequency EPR studies on deuterated and ^{15}N-substituted cyanobacteria.[49−51,53,58]

Using **g** tensor orientation I, we obtain the three-dimensional structure of $P_{700}^{+}A_{1A}^{-}$ in the photosynthetic membrane, as shown in Figure 8b. The structural model is based on the assumption

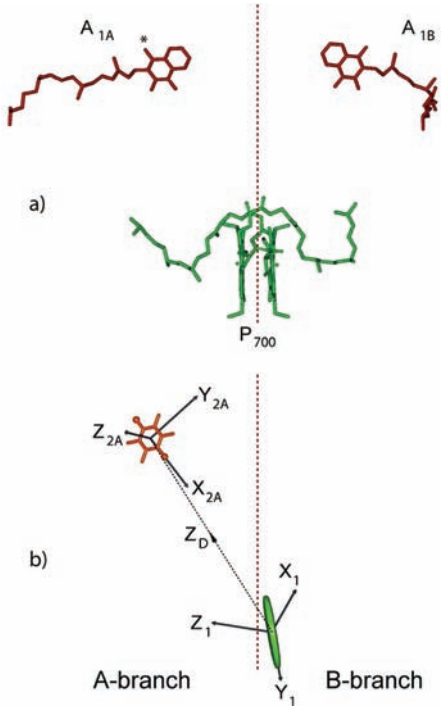

Figure 8. (a) Cofactor arrangement of the ultimate electron donor P_{700} and the phylloquinone acceptors A_{1A} and A_{1B} in photosystem I determined by X-ray crystallography.[1] The figure was generated with Accelrys DS Visualizer 2.0 using the X-ray crystallographic coordinates deposited at Brookhaven data bank under accession number 1JB0, 2001. The direction of view is parallel to the membrane plane. The dotted red line indicates the pseudo-C_2 symmetry axis collinear with the membrane normal. (b) Three-dimensional structure of the A-side radical pair $P_{700}^{+}A_{1A}^{-}$ in photosystem I determined by Q-band quantum oscillations in combination with multifrequency EPR and deuterated wild-type cells of *C. reinhardtii*. The green disk represents chlorophyll *a* in P_{700} coordinated by the PsaB protein subunit. It carries the major part of the unpaired electron spin.[65] $\mathbf{X}_1$, $\mathbf{Y}_1$, $\mathbf{Z}_1$ = principal axis system of the **g** tensor of P_{700}^{+}. $\mathbf{X}_{2A}$, $\mathbf{Y}_{2A}$, $\mathbf{Z}_{2A}$ = principal axis system of the **g** tensor of the reduced A-side quinone A_{1A}^{-}. $\mathbf{Z}_D$ = symmetry axis of the dipolar tensor (interspin vector).

that the major part of the unpaired electron spin in P_{700}^{+} is on the chlorophyll *a* species coordinated by the PsaB protein subunit.[65] Figure 8a depicts the cofactor arrangement of P_{700}, A_{1A}, and A_{1B} as determined by X-ray crystallography. Comparison with Figure 8b reveals that the position of the A-side quinone in both structures is very similar. A minor shift of A_{1A}^{-} of 2.5 Å relative to the position of A_{1A} in the X-ray structure is insignificant in view of the error limits of the quinone shift.[61]

Spatial Structure of the B-Side Radical Pair. To evaluate the spatial structure of $P_{700}^{+}A_{1B}^{-}$, we require the **g** tensor

dx.doi.org/10.1021/ja208806g | J. Am. Chem. Soc. 2012, 134, 5563−5576

orientation of P_{700}^{+} in the B-side radical pair. In principle, this information can be obtained from a high-time-resolution X- and W-band EPR study[25] using a deuterated and ^{15}N-substituted PsaA-M684H mutant. So far, however, this particular mutant has not been prepared.

To proceed, we make the plausible assumption that the **g** tensor orientation of P_{700}^{+} in the B-side radical pair is the same as that in $P_{700}^{+}A_{1A}^{-}$. Thus, by using **g** tensor orientation I (see Table 1, columns 4 and 5)

$$\Phi_1^{Chl} = 183°,\ \Theta_1^{Chl} = 29°,\ \Psi_1^{Chl} = 220°$$

we obtain the three-dimensional structure of $P_{700}^{+}A_{1B}^{-}$ in the photosynthetic membrane, as shown in Figure 9b. The structure

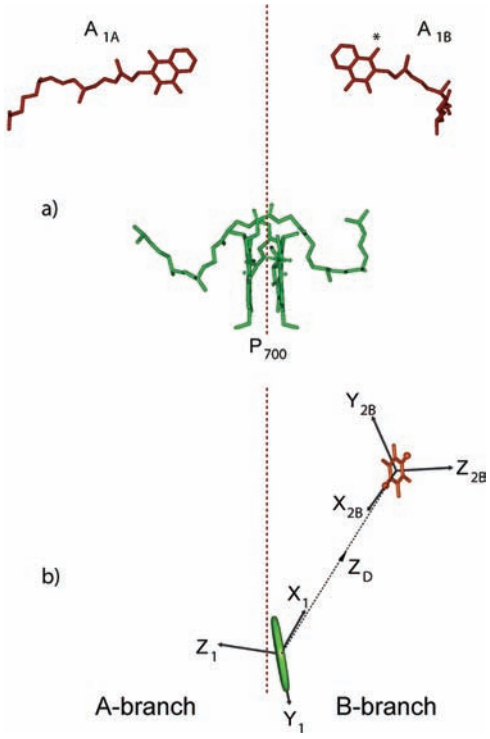

Figure 9. (a) Cofactor arrangement of the ultimate electron donor P_{700} and the phylloquinone acceptors A_{1A} and A_{1B} in photosystem I determined by X-ray crystallography.[1] The figure was generated with Accelrys DS Visualizer 2.0 using the X-ray crystallographic coordinates deposited at Brookhaven data bank under accession number 1JB0, 2001. The direction of view is parallel to the membrane plane. The dotted red line indicates the pseudo-C_2 symmetry axis collinear with the membrane normal. (b) Three-dimensional structure of the B-side radical pair $P_{700}^{+}A_{1B}^{-}$ in photosystem I determined by Q-band quantum oscillations in combination with multifrequency EPR and the deuterated PsaA-M684H mutant of *C. reinhardtii*. The green disk represents chlorophyll *a* in P_{700} coordinated by the PsaB protein subunit. It carries the major part of the unpaired electron spin.[65] $\mathbf{X}_1$, $\mathbf{Y}_1$, $\mathbf{Z}_1$ = principal axis system of the **g** tensor of P_{700}^{+}. $\mathbf{X}_{2B}$, $\mathbf{Y}_{2B}$, $\mathbf{Z}_{2B}$ = principal axis system of the **g** tensor of the reduced B-side quinone A_{1B}^{-}. $\mathbf{Z}_D$ = symmetry axis of the dipolar tensor (interspin vector).

describes the position and orientation of A_{1B}^{-} a few tens of nanoseconds after light-induced charge separation. The new information is based on the analysis of quantum oscillations in combination with two-dimensional correlation spectroscopy and the deuterated PsaA-M684H mutant.

Figure 9a shows the cofactor arrangement of the primary donor P_{700} and the two phylloquinone acceptors A_{1A} and A_{1B} as determined by X-ray crystallography.[1] Comparison with Figure 9b reveals that electron transfer in the PsaA-M684H mutant occurs along the B-branch of the cofactor chain. The notable shift of A_{1B}^{-} of 5.3 Å relative to the position of A_{1B} in the X-ray structure is not critical as it still remains within the error limits of the Q-band study.[61,66] Thus, we have observed the three-dimensional structure of the B-side radical pair $P_{700}^{+}A_{1B}^{-}$ following photoexcitation of PS I in its native membrane.

DISCUSSION

Time-Resolved EPR Spectra of the A- and B-Side Radical Pairs. Analysis of the two-dimensional nutation experiments provides the time evolution of the transverse electron spin magnetization of $P_{700}^{+}A_{1A}^{-}$ and $P_{700}^{+}A_{1B}^{-}$ at equidistant field points covering the total spectral width. Transient spectra can be extracted from such a plot at any given time after the laser pulse. In Figure 10 we depict spin-polarized Q-band EPR

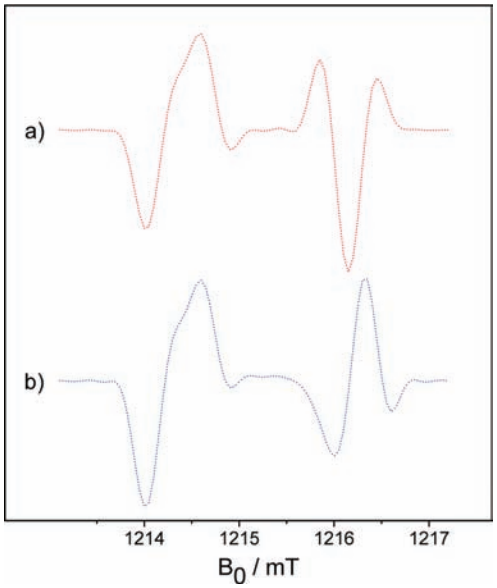

Figure 10. (a) Transient Q-band EPR spectrum of the A-side radical pair $P_{700}^{+}A_{1A}^{-}$ in photosystem I calculated for a delay time of 110 ns after the laser pulse. The underlying Euler angles are summarized in Table 2. (b) Transient Q-band EPR spectrum of the B-side radical pair $P_{700}^{+}A_{1B}^{-}$ in photosystem I calculated for a delay time of 110 ns after the laser pulse. The underlying Euler angles are summarized in Table 1. Analysis reveals that the line shapes of $P_{700}^{+}A_{1A}^{-}$ and $P_{700}^{+}A_{1B}^{-}$ can be rationalized on the basis of their spatial structures determined by Q-band quantum oscillations in combination with high-time-resolution X- and W-band EPR.

spectra of $P_{700}^{+}A_{1A}^{-}$ (Figure 10a) and $P_{700}^{+}A_{1B}^{-}$ (Figure 10b) for a delay time of 110 ns. Comparison reveals that the line shapes of the low-field portion of the radical pair spectra are very similar, whereas the high-field parts are markedly different. How can one rationalize this observation? For convenience, we employ a *stationary* EPR model, in which the *pseudosecular terms of the electron spin–spin interactions* are ignored.[67−69] As a result, light-induced quantum oscillations are neglected. The latter is a reasonable approximation in the present case, since 110 ns after the laser pulse all quantum oscillations have disappeared (see Figures 4 and 7).

According to the stationary model, the line shape of the time-resolved EPR spectrum can be described as the sum of two contributions from the two constituents of the radical pair, P_{700}^{+} and A_{1A}^{-} (A_{1B}^{-}).[67−69] The line shapes of these contributions depend primarily on the orientation of the symmetry axis of the

dx.doi.org/10.1021/ja208806g | J. Am. Chem. Soc. 2012, 134, 5563−5576

Table 3. Orientation of the Symmetry Axis of the Dipolar Tensor (Interspin Vector) in the A- and B-Side Radical Pairs $P_{700}^{+}A_{1A}^{-}$ and $P_{700}^{+}A_{1B}^{-}$ of Photosystem I

interspin vector orientation in the **g** tensor of A_{1A}^{-} (A_{1B}^{-})				interspin vector orientation in the **g** tensor of P_{700}^{+}			
$P_{700}^{+}A_{1A}^{-}$ [a]		$P_{700}^{+}A_{1B}^{-}$ [b]		$P_{700}^{+}A_{1A}^{-}$ [a]		$P_{700}^{+}A_{1B}^{-}$ [b]	
notation[c]	angular value (deg)	notation[c]	angular value (deg)	notation[d]	angular value (deg)	notation[d]	angular value (deg)
Θ_{DA}	71	Θ_{DB}	70	Θ'_{DA}	54	Θ'_{DB}	116
Ψ_{DA}	11	Ψ_{DB}	23	Ψ'_{DA}	246	Ψ'_{DB}	299

[a]Determined using the deuterated wild-type cells of *C. reinhardtii*. [b]Evaluated using the deuterated PsaA-M684H mutant of *C. reinhardtii*. [c]The Euler angles Θ_{DA}, Ψ_{DA}, Θ_{DB}, and Ψ_{DB} transform from the axially symmetric dipolar tensor in the A- or B-side radical pair to the respective magnetic reference system (**g** tensor of A_{1A}^{-} or A_{1B}^{-}). [d]The Euler angles Θ'_{DA}, Ψ'_{DA}, Θ'_{DB}, and Ψ'_{DB} transform from the axially symmetric dipolar tensor in the A- or B-side radical pair to the **g** tensor system of P_{700}^{+}.

dipolar tensor (interspin vector), $P_{700}^{+}-A_{1A}^{-}$ ($P_{700}^{+}-A_{1B}^{-}$), in the **g** tensor system of A_{1A}^{-}, A_{1B}^{-}, or P_{700}^{+}.[67−69] Table 3 summarizes the Euler angles which transform from the axially symmetric dipolar tensor in the A- and B-side radical pairs to the respective magnetic reference system, i.e., the **g** tensor system of A_{1A}^{-}, A_{1B}^{-}, or P_{700}^{+}. Values for these angles were obtained from computer fits of the two-dimensional Q-band EPR experiments.

Inspection of Table 3 reveals that the orientations of the interspin vectors $P_{700}^{+}-A_{1A}^{-}$ and $P_{700}^{+}-A_{1B}^{-}$ are very similar in the **g** tensor principal axes of the respective semiquinone (columns 1−4), consistent with the symmetric arrangement of A_{1A}^{-} and A_{1B}^{-} relative to the membrane normal (see Figures 8b and 9b). This symmetry determines the similar line shapes of the low-field parts of the EPR spectra, where the main contribution is from the quinone member of the spin-correlated radical pair.[23]

The situation is different in the high-field part of the spectra, where the main contribution comes from P_{700}^{+}. In this region, the distinctions between the line shapes of $P_{700}^{+}A_{1A}^{-}$ and $P_{700}^{+}A_{1B}^{-}$ indicate that the orientations of the $P_{700}^{+}-A_{1A}^{-}$ and $P_{700}^{+}-A_{1B}^{-}$ interspin vectors are different in the **g** tensor axes of P_{700}^{+} (Table 3, columns 5−8).[23] This can be verified by inspection of Figures 8b and 9b, which reveal a breaking of the approximate C_2 symmetry of the quinone cofactors in the electronic structure of P_{700}^{+}. Thus, we have rationalized the spin-polarized EPR spectra of $P_{700}^{+}A_{1A}^{-}$ and $P_{700}^{+}A_{1B}^{-}$ on the basis of their spatial structures.

It is important to emphasize that the line shape of the time-resolved EPR spectrum observed with high spectral resolution (achieved here with Q-band EPR and deuterated whole cells of *C. reinhardtii*) provides us with unique information on the geometric arrangement of the cofactors within the spin-correlated radical pair, as demonstrated before[23] to prove bidirectionality of electron transfer in PS I in the fully deuterated cyanobacterium *Synechococcus lividus*. The shape of the time-resolved EPR spectra reported here is very similar to that of spectra recorded at D-band EPR and reported for the spin-correlated radical pair in both the A- and B-branches.[23] This provides strong support for the model that bidirectionality is a general property of the PS I type I reaction center from both prokaryotes and eukaryotes[22,70] and contrasts with the situation for photosystem II and other type II reaction centers, in which electron transfer is highly asymmetric. However, in ref 23, to observe two distinct radical pair spectra, the reducing conditions of the sample had to be varied, which may introduce additional complications in interpretation. The data presented here do not suffer from this possible drawback, as all of the experiments were performed under ambient redox conditions.

Orientation of the Reduced Phylloquinones in their Binding Sites. Analysis of quantum oscillations, observed in two-dimensional Q-band EPR experiments, provides the three-dimensional structure of $P_{700}^{+}A_{1A}^{-}$ and $P_{700}^{+}A_{1B}^{-}$ following photoexcitation of PS I in their native membranes. Figure 8b shows the spatial arrangement of $P_{700}^{+}A_{1A}^{-}$ a few tens of nanoseconds after light-induced charge separation. The structure describes the position and orientation of A_{1A}^{-} in the photosynthetic membrane. Note that values for all eight Euler angles, characterizing the structure of $P_{700}^{+}A_{1A}^{-}$, have been obtained (see Table 2). Our EPR results indicate that the quinone plane of A_{1A}^{-} is inclined by 93° relative to the membrane plane. This value is in substantial agreement with a value of 67° reported in the high-resolution X-ray structure (see Figure 8a, left side).[1] On the basis of the latter study, a detailed model of the A_{1A} binding pocket has been developed.[13] The most striking feature of this model is a single hydrogen bond formed between the C_4 carbonyl group of A_{1A} (asterisk) and the protein backbone (PsaA-L722).[13,60,71−74] The spatial arrangement of A_{1A}^{-}, determined from the experiments in this study and shown in Figure 8b, is consistent with the presence of this single hydrogen bond.

In Figure 9b we depict the three-dimensional structure of the B-side radical pair $P_{700}^{+}A_{1B}^{-}$ following photoexcitation of PS I in its native membrane. Figure 9a shows the cofactor arrangement of P_{700}, A_{1A}, and A_{1B} as determined by X-ray crystallography.[1] The notable shift of A_{1B}^{-} relative to the position of A_{1B} in the X-ray structure can be explained by the error limits of the Q-band study.[61,66] However, while the position of A_{1B}^{-} is compatible with the X-ray structure, the orientation of A_{1B}^{-} appears to be remarkably different. Analysis reveals a major rotation of A_{1B}^{-} relative to its orientation in the crystallographic model. Even with a cautious interpretation of the systematic errors of the Q-band study, such a rotation cannot be reconciled with the X-ray structure.[75] The rotation implies a significant weakening of a hydrogen bond between the C_4 carbonyl group of A_{1B}^{-} (asterisk) and the protein backbone (PsaB-L706) which was postulated on the basis of the crystallographic model.[13] To corroborate this result, we plan to perform pulsed high-field ENDOR experiments on the radical pair intermediates[77] using the deuterated wild-type cells and the deuterated PsaA-M684H mutant of *C. reinhardtii*.

Kinetics of Forward Electron Transfer from A_{1A}^{-} and A_{1B}^{-} to F_X. Combining the analysis of quantum oscillations with two-dimensional correlation spectroscopy, we have determined the structure of the transient intermediates $P_{700}^{+}A_{1A}^{-}$ and $P_{700}^{+}A_{1B}^{-}$ in both branches of the electron transfer chain. A detailed comparison reveals different orientations of A_{1A}^{-} and A_{1B}^{-} in their respective binding pockets. While the orientation of A_{1A}^{-} is compatible with the X-ray structure, A_{1B}^{-} shows a major rotation relative to the crystallographic model. The rotation implies a

dx.doi.org/10.1021/ja208806g | *J. Am. Chem. Soc.* 2012, 134, 5563−5576

significant weakening of a single hydrogen bond between A_{1B}^- and the protein backbone.

One consequence of a weakened hydrogen bond is that the midpoint potential of A_{1B}^- should be more negative than that of A_{1A}^-.[13,78,79] Assuming that the A_1^- to F_X electron transfer is in the normal region of the Marcus curve,[80] a more negative redox potential would lead to an increase in the rate of forward electron transfer.[13] This notion is supported by recent room temperature studies of the kinetics of A_1^- oxidation performed on site-directed mutants, in which the hydrogen-bonded leucine residues on the A- and B-branches were substituted by bulkier residues.[63,81] It was found that the rates of forward electron transfer from A_{1A}^- or A_{1B}^- to F_X were consistently faster than those in the wild type. The acceleration of the oxidation kinetics of A_1^- in these mutants is explained by a weakening of the hydrogen bond between A_1^- and the protein backbone, leading to a more negative midpoint potential of A_1/A_1^-.[63,81]

When the room temperature kinetics of A_1^- oxidation are measured in the wild-type cells of *C. reinhardtii*, the rate of A_{1B}^- is faster by 1 order of magnitude than the rate of A_{1A}^-.[14−16] We suggest that this difference is due to the different orientations of A_{1A}^- and A_{1B}^- in their respective binding sites whereby formation of a strong hydrogen bond from A_1^- to the protein backbone is possible only in case of A_{1A}^-. Thus, the present study sheds new light on the function of the phylloquinone acceptors in PS I.

CONCLUSIONS

We have explored the electron transfer pathways of PS I in whole cells of the deuterated green alga *C. reinhardtii* using high-time-resolution EPR at cryogenic temperatures. Analysis of quantum oscillations, observed in a time-resolved Q-band EPR experiment on the deuterated PsaA-M684H mutant, provides the geometry of the B-side radical pair. The orientation of the **g** tensor of P_{700}^+ in an external reference system is adapted from a time-resolved multifrequency EPR study on deuterated and ^{15}N-substituted cyanobacteria.[25] Thus, we have obtained the three-dimensional structure of the B-side radical pair $P_{700}^+A_{1B}^-$ following photoexcitation of PS I in its native membrane. The structure describes the position and orientation of the reduced B-side quinone A_{1B}^- on a nanosecond time scale after light-induced charge separation. The new structural information is based on the analysis of quantum oscillations in combination with two-dimensional correlation spectroscopy.[24,25,47,49−53]

With these techniques, we have determined the structure of the transient intermediates $P_{700}^+A_{1A}^-$ and $P_{700}^+A_{1B}^-$ in both branches of the electron transfer chain using deuterated wild-type cells of *C. reinhardtii*. A detailed comparison reveals different orientations of A_{1A}^- and A_{1B}^- in their respective binding sites. This difference allows for formation of a strong hydrogen bond from A_1^- to the protein backbone in the case of A_{1A}^- but not in the case of A_{1B}^-. We suggest that this results in the different rates of forward electron transfer from A_{1A}^- or A_{1B}^- to the iron−sulfur center F_X, which differ by a factor of 10. Thus, the present study sheds new light on the function of the phylloquinone acceptors in PS I.

ASSOCIATED CONTENT

Supporting Information

Specification of the magnetic parameters of the A- and B-side radical pairs, additional material characterizing the 32 equivalent representations of the radical pair geometry, further information on the **g** tensor orientation of P_{700}^+ in the A-side radical pair, and assessment of the branching ratio from low-temperature experiments. This material is available free of charge via the Internet at http://pubs.acs.org.

AUTHOR INFORMATION

Corresponding Author

gerd.kothe@physchem.uni-freiburg.de

Present Address

[⊥]Istituto di Biofisica, Consiglio Nazionale delle Ricerche, Via Celoria 26, 20133 Milano, Italy.

Notes

The authors declare no competing financial interest.

ACKNOWLEDGMENTS

We thank George Gaines III for advice on growing fully deuterated cells of *C. reinhardtii* and Seigo Yamauchi for stimulating discussions in the course of the data analysis. Research in the Freiburg laboratories was supported by a grant from the Ministry of Science, Research and the Arts of Baden-Württemberg (24-7532.23-1-11/1). Work at Argonne was funded by the Division of Chemical Sciences, Geosciences and Biosciences, Office of Basic Energy Sciences of the U.S. Department of Energy, through Grant DE-AC02-06CH11357. Work at Queen Mary University of London was supported by grants from the U.K. Biotechnology and Biological Sciences Research Council (BBSRC) (CO0350, CO7809, and B18658) and a European Union TMR Programme (Contract No. FMRX-CT98-0214).

REFERENCES

(1) Jordan, P.; Fromme, P.; Witt, H. T.; Klukas, O.; Saenger, W.; Krauss, N. *Nature* **2001**, *411*, 909−917.

(2) Ben-Shem, A.; Frolow, F.; Nelson, N. *Nature* **2003**, *426*, 630−635.

(3) Deisenhofer, J.; Epp, O.; Miki, K.; Huber, R.; Michel, H. *J. Mol. Biol.* **1984**, *180*, 385−398.

(4) Zouni, A.; Witt, H. T.; Kern, J.; Fromme, P.; Krauss, N.; Saenger, W.; Orth, P. *Nature* **2001**, *409*, 739−743.

(5) Holzwarth, A. R.; Müller, M. G.; Niklas, J.; Lubitz, W. *Biophys. J.* **2006**, *90*, 552−565.

(6) Müller, M. G.; Slavov, C.; Luthra, R.; Redding, K. E.; Holzwarth, A. C. *Proc. Natl. Acad. Sci. U.S.A.* **2010**, *107*, 4123−4128.

(7) Thurnauer, M. C.; Rutherford, A. W.; Norris, J. R. *Biochim. Biophys. Acta* **1982**, *682*, 332−338.

(8) Moënne-Loccoz, P.; Heathcote, P.; Maclauchlan, D. J.; Berry, M. C.; Davis, I. H.; Evans, M. C. W. *Biochemistry* **1994**, *33*, 10037−10042.

(9) Purton, S.; Stevens, D. R.; Muhiuddin, I. P.; Evans, M. C. W.; Carter, S.; Rigby, S. E. J.; Heathcote, P. *Biochemistry* **2001**, *40*, 2167−2175.

(10) Sétif, P.; Mathis, P.; Vängard, T. *Biochim. Biophys. Acta* **1984**, *767*, 404−414.

(11) Santabarbara, S.; Heathcote, P.; Evans, M. C. W. *Biochim. Biophys. Acta* **2005**, *1708*, 283−310.

(12) Rappaport, F.; Diner, B. A.; Redding, K. In *Photosystem I: The Light-Driven Plastocyanin:Ferredoxin Oxidoreductase*; Golbeck, J. H., Ed.; Springer: Dordrecht, The Netherlands, 2006; pp 339−360.

(13) Srinivasan, N.; Golbeck, J. H. *Biochim. Biophys. Acta* **2009**, *1787*, 1057−1088.

(14) Brettel, K. *Biochim. Biophys. Acta* **1997**, *1318*, 322−373.

(15) Joliot, P.; Joliot, A. *Biochemistry* **1999**, *38*, 11130−11136.

(16) Guergova-Kuras, M.; Boudreaux, A.; Joliot, A.; Joliot, P.; Redding, K. *Proc. Natl. Acad. Sci. U.S.A.* **2001**, *98*, 4437−4442.

(17) Bautista, J. A.; Rappaport, F.; Guergova-Kuras, M.; Cohen, R. O.; Golbeck, J. H.; Wang, J. Y.; Béal, D.; Diner, B. A. *J. Biol. Chem.* **2005**, *280*, 20030−20041.
(18) Li, Y.; van der Est, A.; Lucas, M. G.; Ramesh, V. M.; Gu, F.; Petrenko, A.; Lin, S.; Webber, A. N.; Rappaport, F.; Redding, K. *Proc. Natl. Acad. Sci. U.S.A.* **2006**, *103*, 2144−2149.
(19) Byrdin, B.; Santabarbara, S.; Gu, F.; Fairclough, W. F.; Heathcote, P.; Redding, K.; Rappaport, F. *Biochim. Biophys. Acta* **2006**, *1757*, 1529−1538.
(20) Fairclough, W. V.; Forsyth, A.; Evans, M. C. W.; Rigby, S. E. J.; Purton, S.; Heathcote, P. *Biochim. Biophys. Acta* **2003**, *1606*, 43−55.
(21) Santabarbara, S.; Kuprov, I.; Fairclough, W. V.; Purton, S.; Hore, P. J.; Heathcote, P.; Evans, M. C. W. *Biochemistry* **2005**, *44*, 2119−2128.
(22) Santabarbara, S.; Kuprov, I.; Hore, P. J.; Casal, A.; Heathcote, P.; Evans, M. C. W. *Biochemistry* **2006**, *45*, 7389−7403.
(23) Poluektov, O. G.; Paschenko, S. V.; Utschig, L. M.; Lakshmi, K. V.; Thurnauer, M. C. *J. Am. Chem. Soc.* **2005**, *127*, 11910−11911.
(24) Kothe, G.; Thurnauer, M. C. *Photosynth. Res.* **2009**, *102*, 349−365.
(25) Link, G.; Berthold, T.; Bechtold, M.; Weidner, J.-U.; Ohmes, E.; Tang, J.; Poluektov, O.; Utschig, L.; Schlesselman, S. L.; Thurnauer, M. C.; Kothe, G. *J. Am. Chem. Soc.* **2001**, *123*, 4211−4222.
(26) Zech, S. G.; Hofbauer, W.; Kamlowski, A.; Fromme, P.; Stehlik, D.; Lubitz, W.; Bittl, R. *J. Phys. Chem. B* **2000**, *104*, 9728−9739.
(27) Harris, E. H. *The Chlamydomonas Sourcebook: A Comprehensive Guide to Biology and Laboratory Use*; Academic Press: San Diego, CA, 1989.
(28) Wollman, F.-C. *EMBO J.* **2001**, *20*, 3623−3630.
(29) Cherkasov, F. G.; Denisenko, G. A.; Vitol, A. Ya.; L'vov, S. G. In *Proceedings of the XXVIth Congress Ampère on Magnetic Resonance and Related Phenomena*; Salikhov, K. M.; Ed.; Zavoisky Physical-Technical Institute: Kazan, Russia, 1994; Vol. *1*, pp 416−417.
(30) Heinen, U.; Poluektov, O. G.; Stavitski, E.; Berthold, T.; Ohmes, E.; Schlesselman, S. I.; Golecki, J. R.; Moro, G. J.; Levanon, H.; Thurnauer, M. C.; Kothe, G. *J. Phys. Chem. B* **2004**, *108*, 9498−9504.
(31) Laukenmann, K. Ph.D. Thesis, University of Freiburg, 1999.
(32) Marquardt, D. W. *J. Soc. Ind. Appl. Math.* **1963**, *11*, 431−441.
(33) Salikhov, K. M.; Bock, C. H.; Stehlik, D. J. *Appl. Magn. Reson.* **1990**, *1*, 195−211.
(34) Bittl, R.; Kothe, G. *Chem. Phys. Lett.* **1991**, *177*, 547−553.
(35) Kothe, G.; Weber, S.; Bittl, R.; Ohmes., E.; Thurnauer, M. C.; Norris, J. R. *Chem. Phys. Lett.* **1991**, *186*, 474−480.
(36) Zwanenburg, G.; Hore, P. J. *Chem. Phys. Lett.* **1993**, *203*, 65−74.
(37) Kothe, G.; Weber, S.; Ohmes, E.; Thurnauer, M. C.; Norris, J. R. *J. Phys. Chem.* **1994**, *98*, 2706−2712.
(38) Kothe, G.; Weber, S.; Ohmes, E.; Thurnauer, M. C.; Norris, J. R. *J. Am. Chem. Soc.* **1994**, *116*, 7729−7734.
(39) Bittl, R.; van der Est, A.; Kamlowski, A.; Lubitz, W.; Stehlik, D. *Chem. Phys. Lett.* **1994**, *226*, 349−358.
(40) Kothe, G.; Bechtold, M.; Link, G.; Ohmes, E.; Weidner, J.-U. *Chem. Phys. Lett.* **1998**, *383*, 51−60.
(41) Thurnauer, M. C.; Norris, J. R. *Chem. Phys. Lett.* **1980**, *76*, 557−561.
(42) Closs, G. L.; Forbes, M. D. E.; Norris, J. R. *J. Phys. Chem.* **1987**, *91*, 3592−3599.
(43) Buckley, C. D.; Hunter, D. A.; Hore, P. J.; McLauchlan, K. A. *Chem. Phys. Lett.* **1987**, *135*, 307−312.
(44) Weber, S.; Kothe, G.; Norris, J. R. *J. Chem. Phys.* **1997**, *106*, 6248−6261.
(45) Jeschke, G. *J. Chem. Phys.* **1997**, *106*, 10072−10086.
(46) Edmonds, A. R. *Angular Momentum in Quantum Mechanics*; Princeton University Press: Princeton, NJ, 1974; pp 6−8.
(47) Kiefer, A. M.; Kast, S. M.; Wasielewski, M. R.; Laukenmann, K.; Kothe, G. *J. Am. Chem. Soc.* **1999**, *121*, 188−198.
(48) Heinen, U.; Berthold, T.; Kothe., G.; Stavitski, E.; Galili, T.; Levanon., H.; Wiederrecht, G.; Wasielewski, M. R. *J. Phys. Chem. A* **2002**, *106*, 1933−1937.
(49) Thurnauer, M. C.; Poluektov, O. G.; Kothe, G. In *Biological Magnetic Resonance. Very High Frequency ESR/EPR*; Grinberg, O. Y., Berliner, L. J., Eds.; Kluwer/Plenum: New York, 2004; pp 165−206.
(50) Link, G.; Poluektov, O. G.; Utschig, L. M.; Lalevée, J.; Yago, T.; Weidner, J.-U.; Thurnauer, M. C.; Kothe, G. *Magn. Reson. Chem.* **2005**, *43*, 103−109.
(51) Thurnauer, M. C.; Poluektov, O. G.; Kothe, G. In *Photosystem I: The Light-Driven Plastocyanin:Ferredoxin Oxidoreductase*; Golbeck, J. H., Ed.; Springer: Dordrecht, The Netherlands, 2006; pp 339−360.
(52) Heinen, U.; Utschig, L. M.; Poluektov, O. G.; Link, G.; Ohmes, E.; Kothe, G. *J. Am. Chem. Soc.* **2007**, *129*, 15935−15946.
(53) Kothe, G.; Norris, J. R.; Poluektov, O. G.; Thurnauer, M. C. In *Biophysical Techniques in Photosynthesis II*; Aartsma, T. J., Matysik, J., Eds.; Springer: Dordrecht, The Netherlands, 2008; pp 305−323.
(54) van der Est, A.; Prisner, T.; Bittl, R.; Fromme, P.; Lubitz, W.; Möbius, K.; Stehlik, D. *J. Phys. Chem. B* **1997**, *101*, 1437−1443.
(55) Bratt, P. J.; Rohrer, M.; Krystek, J.; Evans, M. C.; Brunel, L.-C.; Angerhofer, A. *J. Phys. Chem. B* **1997**, *101*, 9686−9689.
(56) McMillan, F.; Hanley, J.; van der Weerd, L.; Küpling, M.; Un, S.; Rutherford, A. W. *Biochemistry* **1997**, *36*, 9297−9303.
(57) Käss, H.; Bittersmann-Weidlich, E.; Andréasson, L.-E.; Bönigk, B.; Lubitz, W. *Chem. Phys.* **1995**, *194*, 419−432.
(58) Poluektov, O. G.; Utschig, L. M.; Thurnauer, M. C.; Kothe, G. *Appl. Magn. Reson.* **2007**, *31*, 123−143.
(59) Rigby, S. E. J.; Evans, M. C. W.; Heathcote, P. *Biochemistry* **1996**, *35*, 6651−6656.
(60) Niklas, J.; Epel, B.; Antonkine, M. L.; Sinnecker, S.; Pandelia, M.-E.; Lubitz, W. *J. Phys. Chem. B* **2009**, *113*, 10367−10379.
(61) The error limits for the quinone shift can be estimated from the systematic errors of the Q-band EPR experiments.[52] For both the PsaA-M684H mutant and the wild-type cells, error limits of ±5.5 Å are obtained. This uncertainty results from the fact that EPR does not directly determine the position of the cofactors but only measures angles and distances between them. With a separation of 25 Å between P_{700}^{+} and A_1^{-}, an error of ±9° in the radical pair geometry leads to an uncertainty of ±5.5 Å in the position of A_1^{-}.
(62) Furrer, R.; Thurnauer, M. C. *Chem. Phys. Lett.* **1981**, *79*, 28−33.
(63) Santabarbara, S.; Reifschneider, K.; Jasaitis, A.; Gu, F.; Agostini, G.; Carbonera, D.; Rappaport, F.; Redding, K. E. *J. Phys. Chem. B* **2010**, *114*, 9300−9312.
(64) Klette, R.; Törring, J. T.; Plato, M.; Möbius, K.; Bönigk, B.; Lubitz, W. *J. Phys. Chem.* **1993**, *97*, 2015−2020.
(65) Krabben, L.; Schlodder, E.; Jordan, R.; Carbonera, D.; Giacometti, G.; Lee, H.; Webber, A. N.; Lubitz, W. *Biochemistry* **2000**, *39*, 13012−13025.
(66) At present, we cannot exclude that a minor change of the **g** tensor orientation of P_{700}^{+} in $P_{700}^{+}A_{1B}^{+}$ is responsible for the observed quinone shift.
(67) Stehlik, D.; Bock, C. H.; Petersen, J. *J. Phys. Chem.* **1989**, *93*, 1612−1619.
(68) Kandrashkin, Y. E.; van der Est, A. *Spectrachim. Acta* **2001**, *A57*, 1697−1709.
(69) Dubinskii, A. A.; Perekhodtsev, G. D.; Poluektov, O. G.; Rajh, T.; Thurnauer, M. C. *J. Phys. Chem. B* **2002**, *106*, 938−944.
(70) Santabarbara, S.; Kuprov, I.; Poluektov, O.; Casal, A.; Russell, C. A.; Purton, S.; Evans, M. C. W. *J. Phys. Chem. B* **2010**, *114*, 15158−15171.
(71) Rigby, S. E.; Evans, M. C. W.; Heathcote, P. *Biochim. Biophys. Acta* **2001**, *1507*, 247−259.
(72) Karyagina, I.; Golbeck, J. H.; Srinivasan, N.; Stehlik, D.; Zimmermann, I. *Appl. Magn. Reson.* **2006**, *30*, 287−310.
(73) Stehlik, D. In *Photosystem I: The Light-Driven Plastocyanin: Ferredoxin Oxidoreductase*; Golbeck, J. H., Ed.; Springer: Dordrecht, The Netherlands, 2006; pp 361−386.
(74) Srinivasan, N.; Karyagina, I.; Bittl, R.; van der Est, A.; Golbeck, J. H. *Biochemistry* **2009**, *48*, 3315−3324.
(75) The reason for this deviation is not yet clear. Generally, high-time-resolution EPR provides the orientation of the quinone with a higher precision than X-ray diffraction of reaction center single

crystals,[52] yet the opposite is true for the position of the quinone where X-ray crystallography yields more precise results.[52] Interestingly, in the X-ray structure of PS I at 4 Å resolution, the orientation of the B-side quinone mostly remained undetermined.[76]

(76) Klukas, O.; Schubert, W.-D.; Jordan, P.; Krauss, N.; Fromme, P.; Witt, H. T.; Saenger, W. *Biol. Chem.* **1999**, *274*, 7361−7367.

(77) Poluektov, O. G.; Utschig, L. M. In *The Purple Photosynthetic Bacteria*; Hunter, C. N., Daldal, F., Thurnauer, M. C., Beatty, J. T., Eds.; Advances in Photosynthesis and Respiration, Vol. *28*; Springer: Dordrecht, The Netherlands, 2008; pp 953−973.

(78) O'Malley, P. J. *Biochim. Biophys. Acta* **1999**, *1411*, 101−113.

(79) Ishikita, H.; Knapp, E. W. *J. Biol. Chem.* **2003**, *278*, 52002−52011.

(80) Marcus, R. A.; Sutin, N. *Biochim. Biophys. Acta* **1985**, *811*, 265−322.

(81) Srinivasan, N.; Santabarbara, S.; Rappaport, F.; Carbonera, D.; Redding, K.; van der Est, A.; Golbeck, J. H. *J. Phys. Chem. B* **2011**, *115*, 1751−1759.